Probing the R Lines in Tris(acetylacetonato) Chromium(III) and Tris(3-bromo-acetylacetonato) Chromium(III) by Luminescence and Excitation Line Narrowing Spectroscopy

Hans Riesen*,† and Lucjan Dubicki‡

School of Physical, Environmental and Mathematical Sciences, The University of New South Wales, ADFA, Northcott Drive, Canberra, ACT 2600, Australia, and 36 Slessor Crescent, McKellar, Canberra, ACT 2617, Australia

Received: July 02, 2008

Site-selective and narrowed luminescence and excitation spectra in the region of the $^2E \leftarrow {}^4A_2$ transitions are reported for single crystals of Al(acac)$_3$/Cr(III) and Al(3-Br-acac)$_3$/Cr(III) (where acac is acetylacetonate). The R_2 line is pronounced in the brominated system and displays a comparable oscillator strength as the R_1 line. The ^2E splitting is found to be 138 cm^{-1}, and the $^4A_2$ ground-state splitting is 1.39 cm^{-1}. However, in the case of the Al(acac)$_3$/Cr(III) system the R_2 line is not a distinct feature. We propose that vibronic coupling via a second-order Jahn−Teller effect leads to a redistribution of R_2 intensity over several vibrational sidelines. An upper limit for the R_1 line width $\Gamma_h = 15$ MHz is deduced for the Al(acac)$_3$/Cr(III) 1% system at 1.5 K. This line width is limited by direct and indirect electron-spin−electron-spin interactions. Accurate zero-field splittings (1.20, 1.19, 1.17 cm^{-1}) for the three sites in Al(acac)$_3$/Cr(III) are determined and compared with previously published electron paramagnetic resonance (EPR) data.

1. Introduction

The electronic spectroscopy of the archetypal organometallic tris(acetylacetonato) chromium(III) (Cr(acac)$_3$) complex has received considerable interest over the last 4 decades.[1−12] This complex exhibits interesting electronic features that are based on the d^3 electronic structure and the ligand field of phase-coupled ligators.[9,11,12] In some early work, Orgel proposed that chelate ligands, such as acetylacetonate, may cause a symmetry lowering of the ligand field, by the phase coupling of the pπ orbitals on the coordinating ligands.[13] The highest occupied molecular orbitals (HOMOs) and lowest unoccupied molecular orbitals (LUMOs) of both the acetylacetonate and 3-bromo-acetylacetonate are in-phase and out-of-phase, i.e., of ψ- and χ-type, respectively. The ψ-type bidentate field of the tris complex splits the t_2 orbitals into a_1 and e components, with the e orbitals at higher energy. From the calculation by Atanasov and Schönherr it appears that the energy and splitting of the ^2E multiplet is highly sensitive to the interaction with the phase-coupled frontier orbitals.[9]

It was recognized early that the Cr(acac)$_3$ complex has to be studied in a host lattice in order to avoid intermolecular interactions, e.g., exchange interactions.[2] Suitable crystalline hosts are provided by Al(acac)$_3$ and Ga(acac)$_3$. The low-temperature luminescence spectrum of Al(acac)$_3$/Cr(III) exhibits three pronounced lines at 773.12, 776.43, and 778.43 nm. These lines were originally assigned to the two (nonthermalized) R lines (773.12 and 776.43 nm) and a phonon sideline (778.43 nm), respectively.[2] However, other researchers correctly suggested that the three transitions are due to the R_1 line of crystallographically inequivalent sites in accord with electron paramagnetic resonance (EPR) measurements by Andriessen.[6]

TABLE 1: Measured $^4A_2$ Splittings in Al(acac)$_3$/Cr(III) 1% and Al(3-Br-acac)$_3$/Cr(III) 1% in Units of cm^{-1} [a]

system	this work	EPR result and notation	110 K angles θ, φ, and α (295 K: 31, 13, 94)
Al(acac)$_3$/Cr(III) 1%			
site A	1.19	1.192 (C)	(32, 6, 81)
site B	1.20	1.200 (A)	(31,20,107)
site C	1.17	1.174 (B)	(32,15, 94)
Al(3-Br-acac)$_3$/ Cr(III) 1%	1.39		

[a] The site notation of the EPR work is indicated in parentheses, and the angles are defined in ref 6.

This latter work indicated that Al(acac)$_3$ undergoes a first-order phase transition at 140 ± 1 K where the unit cell triples along the *a*-axis but the space group remains $P2_1/c$. This space group was determined in some early work at room temperature by Morosin.[14] The EPR measurements indicated that the molecules in the lattice are rotated at the phase transition, yielding three distinct sites. The rotations are quantified by the angles θ, φ, and α tabulated in Table 1.[6] Importantly, it was observed that the rhombic parameter *E* significantly increases from 0.0081 to 0.0125, 0.0155, and 0.0148 cm^{-1} upon the phase transition, whereas the other paramagnetic parameters, as defined in the spin-Hamiltonian of eq 1, deviate little from their room temperature values.

$$H(^4A_2) = \mu_B(g_xH_xS_x + g_yH_yS_y + g_zH_zS_z) + D(S_z^2 - 5/4) + E(S_x^2 - S_y^2) \quad (1)$$

EPR experiments also indicated that the $2\bar{A}(\pm 3/2)$ (trigonal notation) lies below the $\bar{E}(\pm 1/2)$ in the $^4A_2$ ground state. We note here that the trigonal notation is not fully justified as the rhombic parameter $E \neq 0$, and hence, significant lower

* Corresponding author. E-mail: h.riesen@adfa.edu.au. Tel.: ++61 (0)2 6268 86 79. Fax: ++61 (0)2 6268 8017.
† The University of New South Wales.
‡ 36 Slessor Crescent.

10.1021/jp805831a CCC: $40.75
Published on Web 09/13/2008

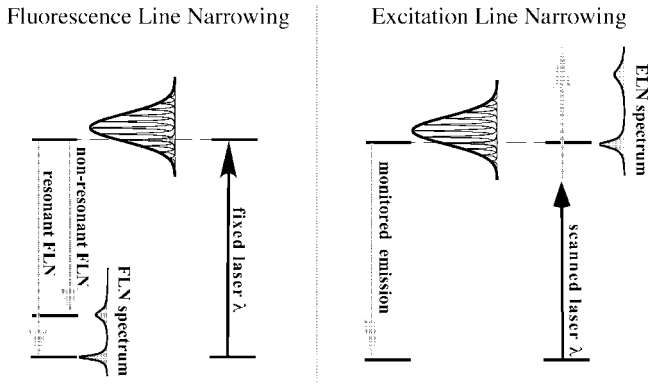

Figure 1. Schematic diagram illustrating the principle of FLN and ELN spectroscopy.

symmetry fields are present at low temperature. From polarized emission spectra Schönherr et al. concluded that the $2\bar{A}$ (^{2}E) is the lower ^{2}E level.[7] From absorption spectra (that were not illustrated) of highly doped crystals it was also purported that the ^{2}E splitting is in the range of 220−290 cm^{-1} in the Ga(acac)$_3$ and Al(acac)$_3$ hosts for the inequivalent molecules.[9] However, on the basis of *g*-factors of the lowest excited state ($|g_\perp| = 1.92$, $|g_\parallel| = 1.60$) obtained by Zeeman and optically detected magnetic resonance measurements and assuming trigonal symmetry for the molecular complexes, Fields et al. suggested that the lowest excited state may be of $^2T_1[\pm 1/2a\mp]$ character.[8]

The present work attempts to address some of these problems and reports on excitation and luminescence line narrowing experiments performed on the Al(acac)$_3$/Cr(III) and Al(3-Br-acac)$_3$/Cr(III) systems. Electronic transitions in the solid state suffer ubiquitously from inhomogeneous broadening.[15] However, selective laser excitation and luminescence monitoring can yield drastically narrowed luminescence and excitation spectra, enabling detailed studies of electronic origins and their vibrational sidelines.[15] In fluorescence (luminescence) line narrowing experiments (FLN) a subset of chromophores is selectively excited by a narrow laser line within the inhomogeneously broadened transition. Narrowed emission from the subset then results. Likewise, in excitation line narrowing (ELN) experiments luminescence of a subset of chromophores is selectively observed with a narrow band-pass (either through a high-resolution monochromator or interferometer) and a narrow-band laser is scanned over the excitation range. The two techniques are schematically illustrated in Figure 1.

2. Experimental Section

Cr(acac)$_3$ was prepared as is described in the literature. Al(acac)$_3$ was obtained from Strem Chemicals. The brominated complexes were prepared as is described in ref 16. Doped crystals of Al(acac)$_3$/Cr(III) 1% and Al(3-Br-acac)$_3$/Cr(III) 1% were grown by slow evaporation of ethanol and toluene solutions.

Nonselective luminescence and excitation spectra were recorded by using an Ar$^+$ laser (Spectra Physics 171) and an Ar$^+$ laser pumped single-frequency Ti:sapphire ring laser (Schwartz Electro-Optics), respectively, as the excitation source. The luminescence was dispersed by a Spex 1404 0.85 m double monochromator equipped with 1200 grooves/mm gratings blazed at 750 nm. The light was detected using a red-sensitive RCA31034 photomultiplier, and the signal was processed by a Stanford Research Systems SRS530 lock-in amplifier. In selective experiments the laser and the luminescence were passed through the same optical chopper wheel with a phase difference of 180° allowing measurements of transitions resonant with the laser. The same method was also applied in high-resolution FLN experiments where a scanning plane-parallel Fabry−Perot interferometer (Burleigh RC-110) was used. In the FLN experiments the signal was processed by either the SRS530 lock-in amplifier or a Tektronix TDS620 digital oscilloscope. Samples were cooled by the flow tube technique or by a liquid helium immersion cryostat built in the laboratory. The laser wavelength was monitored using a Burleigh WA-2000jr wavemeter, and the Ti:sapphire laser was scanned by a computer-controlled stepper motor.

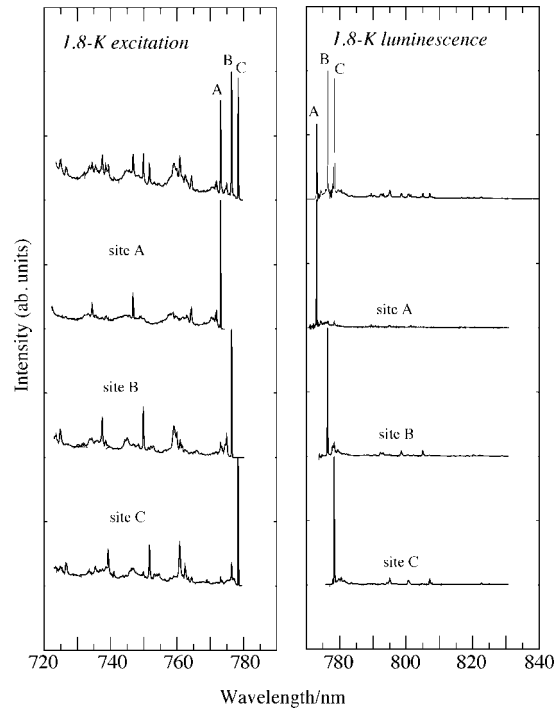

Figure 2. Nonselective and selective luminescence and excitation spectra of Al(acac)$_3$/Cr(III) 1% at 1.8 K in the region of the $^2E \leftarrow {}^4A_2$ transition. The top traces show the nonselectively excited luminescence spectrum (10 mW Ar$^+$ laser all lines excited) and the nonselectively monitored excitation spectrum (750 nm blazed grating in zero order with a 715 nm cutoff filter, 180° phase shift between laser light and luminescence). The selective excitation spectra were monitored with a bandwidth of 0.05 nm at the following: site A 773.12, site B 776.43, and site C 778.43 nm. The selective luminescence spectra were excited at the following: site A 773.04, site B 776.36, and site C 778.43 nm.

3. Results and Discussion

3.1. The ^{2}E Splitting: The Search for the Elusive R_2 Line. Figure 2 shows nonselective and selective excitation and luminescence spectra of Al(acac)$_3$/Cr(III) 1% at low temperatures. The spectra unequivocally confirm that the three pronounced transitions are the electronic origins of three crystallographically inequivalent sites, labeled A, B, and C. A peculiar feature in the excitation spectra is the conspicuous absence of a prominent R_2 feature, i.e., a feature with an intensity comparable to R_1. In contrast, the nonselective and selective excitation spectra of Al(3-Br-acac)$_3$/Cr(III) 1% displayed in Figure 3 show a transition with a comparable intensity as R_1 at ∼138 cm^{-1} higher in energy. This behavior is reminiscent of that encountered in hexaaquachromium(III) complexes where the R_2 line is sometimes a distinct feature and sometimes hard to identify.[17] As follows from Figures 2 and 3, the vibrational coupling is significantly stronger in the excited state compared

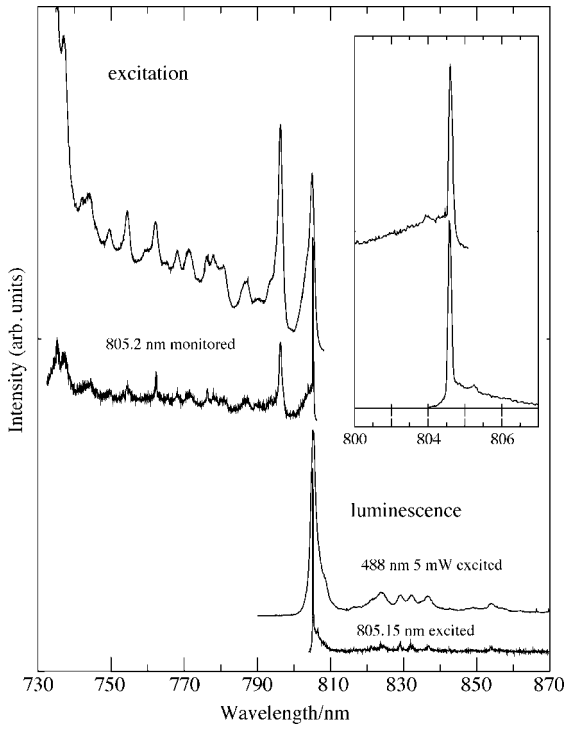

Figure 3. Nonselective and selective luminescence excitation spectra of Al(3-bromo-acac)$_3$/Cr(III) 1% at 10 K in the region of the $^2E \leftarrow {}^4A_2$ transitions. The nonselective and selective luminescence spectra were excited at 488 (5 mW) and 805.15 nm (20 mW), respectively. The total luminescence was monitored in the nonselective excitation spectrum (RG715 cutoff filter, 180° phase shift between the laser light and the luminescence). In the selective excitation spectrum the luminescence was resonantly monitored at 805.2 nm. The inset shows the selective spectra in the region of the R_1 line.

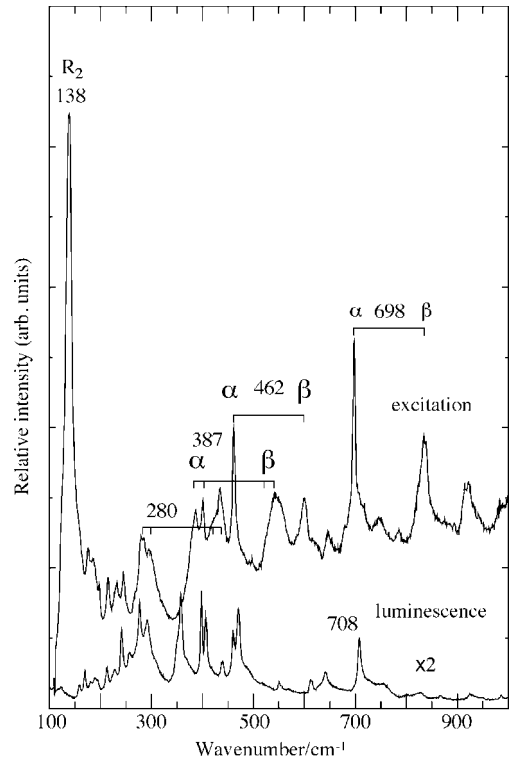

Figure 4. Comparison of the vibrational sidelines observed in narrowed luminescence and excitation spectra of Al(3-bromo-acac)$_3$/Cr(III) 1% at 10 K. The spectra are normalized to the intensity of the R_1 line (see Figure 3 for the relative intensities of R_1 and R_2). Sidelines in the excitation spectrum based on the R_1 and R_2 line are denoted with α and β, respectively.

to the ground state, i.e., vibrational sidelines carry more intensity in the excitation spectra. Also, the pronounced long-wave phonon wing as observed in narrowed luminescence and excitation spectra shown in Figure 3 is an interesting feature. These wings are the composite of the true phonon wing (PW) of the resonantly excited centers and broad luminescence that gets nonresonantly excited via the phonon wing. The observed Debye−Waller factor α′ is thus smaller than the true value defined in eq 2 where I_{ZPL} and I_{PW} stand for the oscillator strength of the zero phonon line and the phonon wing, respectively. The observed and real value have the approximate relationship $\alpha' \approx \alpha^2$, if the excited-state and ground-state Debye−Waller factors are approximately the same.[18] The observed Debye−Waller factor at 10 K is $\alpha' = 0.40$ and 0.31 in the ground and lowest excited state, respectively. Thus, the real values are about $\alpha \approx 0.63$ and 0.56, again indicating a stronger vibronic coupling in the excited state.

$$\alpha(T) = \frac{I_{ZPL}(T)}{I_{ZPL}(T) + I_{PW}(T)} \qquad (2)$$

Usually, the electron−phonon coupling in the R lines of chromium(III) complexes is very low as, in first-order approximation, these transitions are simple spin-flips within the $(t_2)^3$ electronic configuration. Consequently, the Debye−Waller factor is in most cases close to unity. The present systems appear to be subject to an electron−phonon coupling strength which is comparable to that of $\pi\pi^*$ excitations of organic molecules. For example, we have determined a Debye−Waller factor of $\alpha \approx 0.6$ for the ligand-centered $^3\pi-\pi^*$ transition Ru(II) tris(3,3′-biisoquinoline).[19] This value is almost identical to the one determined for Al(3-Br-acac)$_3$/Cr(III) 1% in this work (this is further discussed below).

Figures 4 and 5 present a detailed comparison of vibrational sidelines observed in narrowed excitation and luminescence spectra of Al(3-Br-acac)$_3$/Cr(III) 1% and Al(acac)$_3$/Cr(III) 1%, respectively. In the case of Al(3-Br-acac)$_3$/Cr(III) the transition at 138 cm^{-1} is clearly the most pronounced feature in the displayed energy range of the excitation spectrum shown in Figure 3, and it seems safe to assign this transition to the R_2 line of this complex. From the selective excitation spectrum (see Figures 3 and 4) it follows that the ^2E splitting in the complex is relatively poorly correlated and the R_2 line narrows only by 11 cm^{-1} from $\Gamma_{inh} \approx 28$ to 17 cm^{-1}. This is not surprising as the in-phase coupling of frontier orbitals in the present case will be strongly dependent on the exact ligand geometry, and hence, the relevant parameter $e_\pi(\psi)$ and thus the energies of the ^2E levels are highly susceptible to lattice imperfections.

Figure 4 illustrates that the vibrational coupling in the excited state is stronger than in the $^4A_2$ ground state, i.e., vibrational sidelines carry more intensity in excitation than in luminescence. Although many vibrational sidelines are observed both in excitation and in luminescence there are exceptions; for example, the 358 cm^{-1} vibrational sideline in luminescence is absent in the excitation spectrum. Most vibrational modes that are present in both spectra are subject to slight reductions of their frequency in the excited state in accord with expectations. For example, the pronounced sideline at 698 cm^{-1} in excitation corresponds to the vibrational sideline at 706 cm^{-1} in luminescence. In the Al(acac)$_3$/Cr(III) 1% spectra (Figure 5) one can again recognize that low-energy lattice modes (<50 cm^{-1}) couple relatively strongly to the R_1 line. Because of some overlap of the electronic

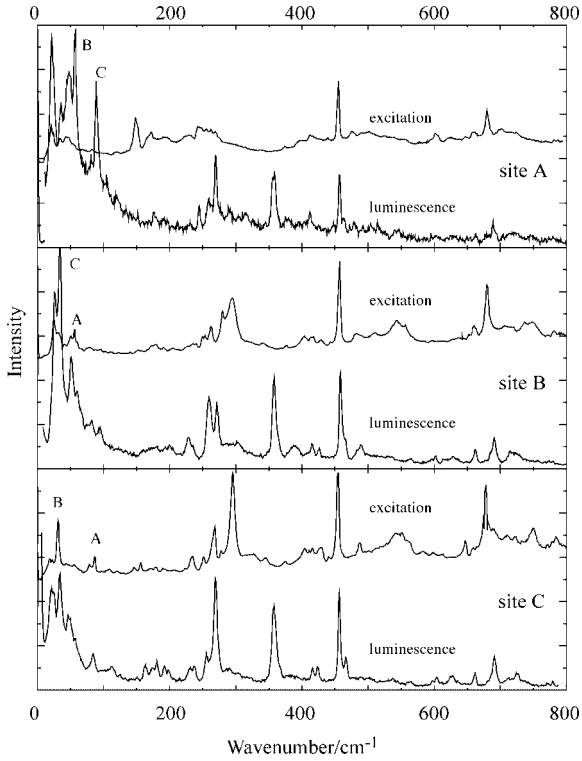

Figure 5. Comparison of the vibrational sidelines in luminescence and excitation of Al(acac)$_3$/Cr(III) 1% at 1.8 K. The spectra are normalized by the 456 cm^{-1} vibrational sideline. Transitions labeled with A, B, and C are minor contributions to some nonselective excitation or luminescence monitoring via vibrational sidelines.

origins with vibrational sidelines, the selectivity is not 100% for the luminescence and excitation spectra of sites A and C, respectively, and both the excitation and luminescence for site B. However, the selective excitation spectrum of site A and the selective luminescence spectrum of site C are pure. Again, the 358 cm^{-1} mode in luminescence is absent in excitation. In contrast the 457 cm^{-1} mode is a pronounced sideline in excitation and luminescence. There is no pronounced transition in the excitation spectra of the three sites that can unambiguously be assigned to the R_2 line.

Moreover, there is definitely no transition in the 100−200 cm^{-1} region for sites B and C that can be assigned to R_2. In the excitation spectrum of site A there is a transition at 150 cm^{-1} that is absent in luminescence. This transition is a possible candidate for R_2 of site A although its intensity is still very low compared to R_1. The main argument for such an assignment would be the fact that this line is not observed in the spectra of sites B and C. However, there seems to be some extra intensity in the 250 cm^{-1} region for site A. In the case of site B the most conspicuous transition, that is absent in luminescence, is the 281−294 cm^{-1} band. This also applies for site C, but in this case the 294 cm^{-1} transition is significantly narrower. There appears to be no vibrational sideline in this region for site A. The 150, 281/294, and 294 cm^{-1} transitions of sites A, B, and C, respectively, appear to have a vibrational sideline at 456 cm^{-1}, indicating that these lines may indeed be due to R_2. The question then remains why the R_2 transition is so weak and apparently drastically different for site A compared with sites B and C. As is indicated above the energy and splitting of the ^{2}E multiplet is highly sensitive to the geometry of the phase-coupled ligators. This explains the very high intensity of the vibrational sidelines and the low Debye−Waller factor for the long-wave phonon wing. Hence, it is possible that vibronic coupling redistributes some of the R_2 intensity onto vibrational sidelines since the energy of the higher lying ^{2}E level may be close to vibrational excitations. The nonzero value of the parameter E in EPR experiments indicates that the actual symmetry of the complex is not trigonal; it is possible that through vibronic coupling the symmetry reduction is much more effective in the ^{2}E excited state, i.e., it is possible that the system is subject to a dynamic Jahn−Teller effect.

It is possible for the half-filled ^{2}E(t_2^3) multiplet to have a Jahn−Teller interaction that becomes large for complexes with large diagonal trigonal fields, v. The second-order Jahn−Teller effect will involve the perturbation $\mathbf{H}_{trig} \times \mathbf{H}_{vib}$, where $\mathbf{H}_{vib} = V(T_2)\mathbf{Q}(T_2)$, $\mathbf{H}_{trig}$ is the Hamiltonian for the trigonal field,

$$V(T_2) = \frac{\partial \mathbf{H}_{trig}}{\partial \mathbf{Q}(T_2)} \tag{3}$$

and the intermediate state is ^{2}T$_2$(t_2^3). If we use the approximation

$$\langle {}^2E|V(T_2)|{}^2T_2\rangle = \langle {}^2E|\frac{\partial \mathbf{H}_{trig}}{\partial \mathbf{Q}(T_2)}|{}^2T_2\rangle \cong \frac{\partial}{\partial \mathbf{Q}(T_2)}\langle {}^2E|\mathbf{H}_{trig}|{}^2T_2\rangle = \frac{\partial}{\partial \mathbf{Q}(T_2)}\left(\frac{\sqrt{6}}{3}v\right) \tag{4}$$

then the effective Jahn−Teller coupling will be approximately proportional to the square of v. Hence all trigonal Cr(III) complexes with large v will have a large second-order Jahn−Teller (JT) coupling in the ^{2}E(t_2^3) multiplet. Equation 4 indicates that the most active modes are those that modulate the trigonal field v and therefore include not only skeletal vibrations but also vibrations localized on the ligand.

For Cr(acac)$_3$ the large v arises from the large energy difference between HOMOs ψ (in-phase) and χ (out-of-phase). This energy gap is the result of π-bonding within the chelate ring and should be modulated most strongly by the ring modes of acac$^-$. We suggest that the ring mode at ≈1550 cm^{-1} is the primary JT vibration. There will be many other chelate vibrations that modulate the trigonal field. In particular vibrations that deform or fold the chelate ring will be JT-active. Among the skeletal (metal−ligand) vibrations, the bending Q(T_{2g}) vibration which changes the metal chelate bite angle should be JT-active; this mode occurs at 358 cm^{-1} and is seen in luminescence but is absent in the excitation spectrum.

Low energy vibrations that mix with the JT-active mode through hydrogen bonding may also couple to the ^{2}E electronic levels, and it is not surprising that the Debye−Waller factor α is small.

Thus, the ^{2}E(t_2^3) multiplet in Cr(acac)$_3$ is subject to a multimode JT interaction and the distribution of the electronic character of R_1 and R_2 lines will be complex. Even for the bromo complex the transition energy of the clearly resolved R_2 line may not be the energy that should be used in a conventional ligand field calculation. The bromine substitution in the apical position of the chelate will tend to reduce folding and hence increase π-bonding within the ring. This may result in a larger trigonal field v and may increase the π covalency of the metal−ligand bond and generate a larger off-diagonal trigonal field.

3.2. The $^4A_2$ Zero-Field Splitting as Observed in High-Resolution FLN Spectra. Figure 6 shows the FLN spectrum of Al(3-Br-acac)$_3$/Cr(III) as observed with resonant excitation into the R_1 line. The zero-field splitting (ZFS) of the $^4A_2$ ground state is much smaller than the inhomogeneous width $\Gamma_{inh} \sim 25$ cm^{-1} of this transition. As a consequence, chromophores can have both the $^2E \leftarrow {}^4A_2(\pm 3/2)$ and the transition $^2E \leftarrow {}^4A_2(\pm 1/$

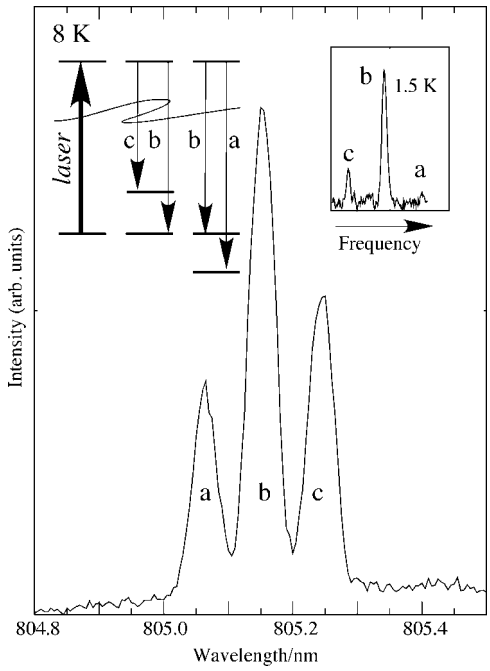

Figure 6. Narrowed luminescence spectrum of Al(3-bromo-acac)$_3$/Cr(III) 1% in the region of the electronic origin (R_1) at 8 K. The line width is limited by the resolution of the monochromator. The inset shows the spectrum at higher resolution at 1.5 K (as observed through the Fabry−Perot interferometer).

2) in resonance with the laser, and a three-line pattern emerges. This is schematically illustrated in Figure 6. The spectra shown in Figure 6 are instrumentally limited. FLN experiments for the Al(acac)$_3$/Cr(III) 1% system are illustrated in Figure 7. The inhomogeneous broadening is relatively low in this system, and the $^4A_2$ splitting leads to a shoulder in the nonselective spectrum. The FLN trace measured with a free spectral range of 53 GHz clearly resolves the ZFS. In this case the resonant excitation of the $^2E \leftarrow {}^4A_2(\pm 3/2)$ transition is selective because of the low inhomogeneous broadening, and only a small fraction of chromophores has their $^2E \leftarrow {}^4A_2(\pm 1/2)$ transition at the laser wavelength.

The lower panel of Figure 7 shows the $^2E \leftarrow {}^4A_2(\pm 3/2)$ transition at high resolution using a FSR of 2.98 GHz. The experimental and instrumental line widths are comparable. The experimental line shape can be described by a convolution of the instrumental line shape with a Lorentzian line with $\Gamma = 30$ MHz. This indicates an upper limit for the homogeneous line width of the $^2E \leftarrow {}^4A_2(\pm 3/2)$ transition of 15 MHz (= 1/2000 cm^{-1}), which is still orders of magnitude above the lifetime-limited line width. The dominant contributions to this relatively large width are direct and indirect electron-spin−electron-spin interactions.[20]

FLN measurements allow very precise determinations of ZFS if the FSR is known accurately. The present measurements also allow the assignment of the sites identified in EPR work to the sites observed in the optical spectroscopy. The results are summarized in Table 1.

The origin of the large zero-field splitting, $D(^4A_2) \approx 1.2$ cm^{-1}, for Al(acac)$_3$/Cr^{3+}, has remained an unresolved problem. Within the conventional ligand field model, $D(^4A_2)$ is mainly determined by the off-diagonal trigonal field v'. However, it is necessary to have accurate values for the average spin−orbit coupling, $\zeta = {}^1/_3(\zeta_x + \zeta_y + \zeta_z)$. The early EPR studies[22,23] gave average g-values $g(^4A_2) = 1.982$ for Al(acac)$_3$/Cr^{3+}. The perturbation expression for the g-shift is

$$g \approx 2.0023 - \frac{8\zeta k}{3\Delta} \quad (5)$$

where Δ is the cubic field and k is the orbital reduction parameter. If we use[9] $\Delta \approx 18\,700$ cm^{-1} and the approximation $\zeta \approx \zeta_0 k$, where ζ_0 is the free-ion spin−orbit coupling constant for Cr^{3+}, then eq 5 gives $\zeta \approx 200$ cm^{-1} and $k \approx 0.72$. The observed $D(^4A_2)$ can then be reproduced by a ligand field calculation provided $v' \approx 1500$ cm^{-1}. A lower value $v' \approx 1200$ cm^{-1} is obtained if we use $\zeta \approx 230$ cm^{-1}.

It should be noted that the $^4T_1{}^a \leftarrow {}^4A_2$ absorption in Cr(acac)$_3$ is not resolved and overlaps with a charge-transfer transition. The $R_1(^2E \leftarrow {}^4A_2)$ energy depends not only on the Racah parameters but also on the trigonal and rhombic field that operate within the t_{2g} subshell. The multimode vibronic interactions within the ^2E multiplet complicate the determination of v. Consequently, there is a lack of precision in all the ligand field calculations.

The oxygen atoms in Cr(acac)$_3$ have very little trigonal distortion. The observed[14] twist angle, $\Delta\varphi = 61.2°$, and the polar compression angle, $\theta = 54.5°$, are very close to the octahedral values, $\Delta\varphi_0 = 60°$ and $\theta_0 = 54.7°$. The origin of the large v' field is particularly intriguing.

Previous workers[9] have suggested that v' may not be large and that the observed $D(^4A_2)$ is due to trigonal anisotropy in ζ that results from the large anisotropy in ψ and χ covalency. Such a mechanism may indeed contribute to $D(^4A_2)$, but we now show that the microscopic ligand field model (AOM) can account for a *major portion* of the estimated v' and the observed $D(^4A_2)$.

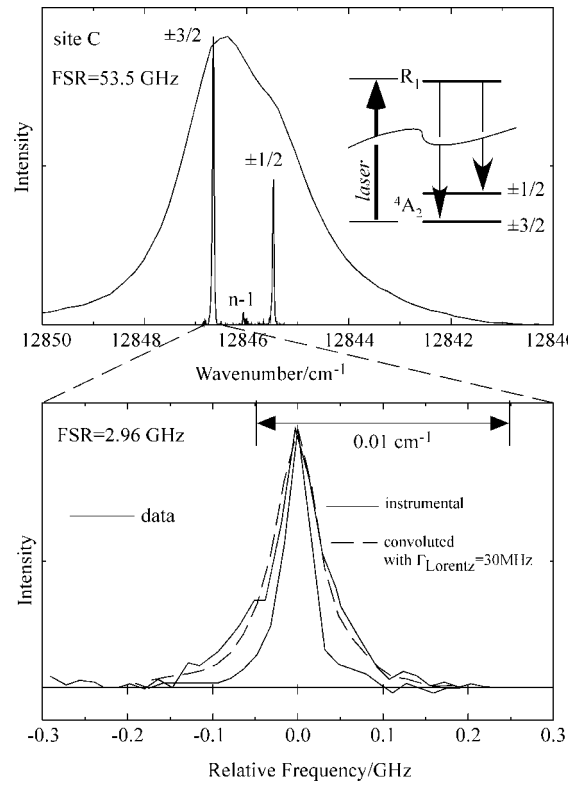

Figure 7. Narrowed luminescence spectrum of site C in Al(acac)$_3$/Cr(III) 1% in the region of the electronic origin (R_1) at 1.8 K. The line width is limited by the resolution of the interferometer. The upper and lower panels show the spectrum obtained with a free spectral range (FSR) of 53.5 and 2.96 GHz, respectively. The $R_1(\pm 3/2)$ line in the lower panel was fitted by a convolution of the instrumental line shape with a Lorentzian of 30 MHz width.

TABLE 2: Calculated Hybridization Coefficients and the Tilt of the Lone Pair for a Given Value of n_{OC}

n_{OC}	n_{OCr}	n_{LP}	$t_{\|\|}$ (deg)[a]
1.0	2.77	3.26	19.4
2.0	1.39	3.04	29.2
3.0	0.92	3.34	34.7

[a] $t_{\|\|} = \angle \mathrm{CrO}h_{LP} - 90$.

In the planar acac$^-$ ligand the oxygen atom prior to bonding with the Cr^{3+} ion has three hybrid orbitals within the plane of the chelate, two lone pairs and a hybrid that binds to the carbon atom. Perpendicular to the plane is a pure 2π orbital that forms strong π bonds. We assume that the coordination of such a ligand to Cr^{3+} will produce extensive electronic relaxation within the two lone pairs so that the Cr−O bond has axially symmetric charge density and all the misalignment is "transferred" to the remaining lone pair.

This model gives a single misaligned lone pair (LP) whose orientation and hybridization is determined by the angle ∠CrOC and the normalization and orthogonality conditions for the four orbitals on the oxygen atom, h_{OCr}, h_{OC}, h_{LP}, and $p_\perp$, where $h = N[(2s) + \sqrt{n}(2p)]$.[24]

In this case a unique solution is not possible, and it is necessary to specify one of the hybridization coefficients. We chose n_{OC}, which gives the π character (sp^n) in the h_{OC} orbital.

Table 2 gives the calculated hybridization coefficients for the oxygen atom in $Cr(acac)_3$, where $\angle \mathrm{CrOC} = 126.9°$.[14] The angle $t_{\|\|}$ is the tilt of the lone pair from the aligned position where h_{LP} is perpendicular to the CrO vector.

For a single misaligned orbital with tilt angle $t_{\|\|}$ the microscopic model gives the bonding parameter

$$e_{\sigma\pi}(\|) = -\frac{1}{2}\sin(2t_{\|\|})\sqrt{e_\pi(\mathrm{LP})^{\mathrm{cov}} \times e_\sigma(\mathrm{LP})^{\mathrm{cov}}} \qquad (6)$$

The AOM parameters e_σ, $e_\pi(\perp)$, $e_\pi(\|)$, $e_{\sigma\pi}(\perp)$, and $e_{\sigma\pi}(\mathrm{II})$ are symmetry parameters which include both electrostatic and covalency interactions. We assume that the principal electrostatic contribution to the metal−ligand bonding is an effective point charge on the ligand. A point charge generates σ and π interactions with axial symmetry, $e_\pi^{\mathrm{e}}(\perp) = e_\pi^{\mathrm{e}}(\|) = e_\pi^{\mathrm{e}}$, and will not contribute to $e_{\sigma\pi}$ so that

$$e_{\sigma\pi} = e_{\sigma\pi}{}^{\mathrm{cov}} \propto \sqrt{e_\sigma{}^{\mathrm{cov}} \times e_\pi{}^{\mathrm{cov}}} \qquad (7)$$

for a single misaligned orbital. For complexes with near-octahedral values for $\Delta\varphi$ and θ, the cubic field Δ is related to the AOM parameters

$$\Delta = 3e_\sigma - 2e_\pi(\perp) - 2e_\pi(\|) \propto 3(e_\sigma^{\mathrm{cov}} + e_\sigma^{\mathrm{e}}) - 2e_\pi(\perp)^{\mathrm{cov}} - 2e_\pi(\|)^{\mathrm{cov}} - 4e_\pi^{\mathrm{e}} \qquad (8)$$

and for complexes with in-phase coupling

$$2e_\pi(\perp) = e_\pi(\psi) + e_\pi(\chi) \qquad (9)$$

We assume that more oxygen 2p will be used in forming the strong O−C σ bond and, from Table 2, $t_{\|\|}$ should be at least 29°. The lone pair is essentially an sp^3 hybrid.

In β alums, the Cr^{3+} ion is coordinated with planar OH_2 ligands and $e_\pi(\perp) - e_\pi(\|) \approx 1000\ \mathrm{cm}^{-1}$.[25] Applying the point charge approximation, we obtain $e_\pi(\perp) - e_\pi(\|) \approx e_\pi(\perp)^{\mathrm{cov}}$. Although the lone pair in acac$^-$ has some σ character, the oxygen atom has more electron charge than the "neutral" oxygen in alums. Consequently, $e_\pi{}^{\mathrm{cov}}$ in eq 6 could be as large as 1000 cm^{-1}.

It is possible to get agreement with the observed $e_{\sigma\pi}$ in α alums[25] by using $e_\sigma{}^{\mathrm{cov}} \approx 5000\ \mathrm{cm}^{-1}$ and $e_\pi{}^{\mathrm{cov}} \approx 1000\ \mathrm{cm}^{-1}$. If we use these values and $t_{\|\|} \approx 29°$ for $Cr(acac)_3$, then eq 6 gives $e_{\sigma\pi}(\|) = -948\ \mathrm{cm}^{-1}$. Since the oxygen atoms are in near-octahedral positions, $v' = -\sqrt{6}/2e_{\sigma\pi}(\|) \approx +1200\ \mathrm{cm}^{-1}$.

$e_\sigma{}^{\mathrm{cov}}$ may be larger in the $Cr(acac)_3$, and thus a value of $v' \approx +1500\ \mathrm{cm}^{-1}$ (see above) is possible.

The bromination of the acac$^-$ ligands tends to stabilize the plane geometry resulting in a larger value of the diagonal trigonal field parameter v (see above). Quantum chemical calculations at semiempirical and density-functional levels[26] indicate that the splitting of the t_{2g} subshell is very sensitive to the orientation/folding of the ligands. For example, in-phase folding of the ligands (D_3 to C_3 point symmetry reduction) reduces this splitting by almost a factor of 2. The lower R_1 energy of $Cr(Br\text{-}acac)_3$ may be due to both a reduction in the Racah parameters and an increase in v. An increase in σ and π covalency will amplify the off-diagonal field v' and hence increase $D(^4A_2)$ (see eq 6).

4. Conclusions

Site-selective excitation and luminescence spectra provide some evidence that the R_2 line in $Al(acac)_3/Cr(III)$ is in the vicinity of 150−300 cm^{-1}. However, it appears that some of its intensity is redistributed over several vibrational sidelines. The $Al(3\text{-}Br\text{-}acac)_3/Cr(III)$ system provides a much clearer case, and the ^2E R_2 line can be identified at 138 cm^{-1} higher in energy. Since the two systems are very similar and the energy of the luminescent multiplet is comparable we conclude that the assignment by Fields et al.[8] of the lowest excited levels to $^2T_1[\pm 1/2a\mp]$ in the $Al(acac)_3/Cr(III)$ system is incorrect and that these levels are indeed as well due to the ^2E state. The g-factors observed by Fields et al. suggest significant low-symmetry field contributions. Related effects were observed in symmetry reduction by amorphous environments.[21] The increase of the E parameter upon the phase transition is in accord with this idea. Line-narrowing experiments allow an accurate determination of the zero-field splittings, and it is possible to correlate the optical sites with the sites and their geometry as determined by EPR spectroscopy. An upper limit of the line width of 15 MHz is observed for the R_1 line, and this width is most likely limited by electron-spin−electron-spin interactions since relatively high dopant concentrations of ca. 1% were used in the present experiments.

The extensive vibronic coupling in the $^2E(t_2^3)$ multiplet is a consequence of a second-order JT interaction that has an approximate quadratic dependence on the magnitude of the v trigonal field.

Acknowledgment. We thank the Australian Research Council for financial support of this work.

References and Notes

(1) (a) Forster, L. S.; DeArmond, K. *J. Chem. Phys.* **1961**, *34*, 2193. (b) Armendarez, P. X.; Forster, L. S. *J. Chem. Phys.* **1964**, *40*, 273.
(2) Courtois, M.; Forster, L. S. *J. Mol. Spectrosc.* **1965**, *18*, 396.
(3) Targos, W.; Forster, L. S. *J. Chem. Phys.* **1966**, *44*, 4342.
(4) Krause, R. A.; Trabjerg, I.; Ballhausen, C. J. *Acta Chem. Scand.* **1970**, *24*, 593.
(5) Norden, B. *Inorg. Nucl. Chem. Lett.* **1975**, *11*, 387.
(6) Andriessen, W. T. M. *J. Phys. Chem. Solids* **1976**, *37*, 189.
(7) Schönherr, T.; Eyring, G.; Linder, R. *Z. Naturforsch., A: Phys., Phys. Chem., Kosmophys.* **1983**, *38A*, 736.
(8) (a) Fields, R. A.; Haindl, E.; Winscom, C. J.; Khan, Z. H.; Plato, M.; Möbius, K. *J. Chem. Phys.* **1984**, *80*, 3082. (b) Fields, R. A.; Winscom, C. J.; Haindl, E.; Plato, M.; Möbius, K. *Chem. Phys. Lett.* **1986**, *124*, 121.
(9) Atanasov, M.; Schönherr, T. *Inorg. Chem.* **1990**, *29*, 4545.

(10) Juban, E. A.; McClusker, J. K. *J. Am. Chem. Soc.* **2005**, *127*, 6857.
(11) Ceulemans, A.; Dendooven, M.; Vanquickenborne, L. G. *Inorg. Chem.* **1985**, *24*, 1153.
(12) Schönherr, T.; Atanasov, M.; Schmidtke, H.-H. *Inorg. Chim. Acta* **1988**, *141*, 27.
(13) Orgel, L. E. *J. Chem. Soc.* **1961**, 3683.
(14) Morosin, B. *Acta Crystallogr.* **1965**, *19*, 131–137.
(15) (a) Riesen, H. *Coord. Chem. Rev.* **2006**, *250*, 1737. (b) Riesen, H. *Struct. Bonding (Berlin)* **2004**, *107*, 179. (c) Krausz, E.; Riesen, H. In *Inorganic Electronic Structure and Spectroscopy*; Solomon, E. I., Lever, A. B. P., Eds.; John Wiley: New York, 1999; Vol. I, pp 307−352.
(16) Collman, J. P.; Moss, R. A.; Maltz, H.; Heindel, C. C. *J. Am. Chem. Soc.* **1961**, *83*, 531–534.
(17) Riesen, H.; Dubicki, L. *Inorg. Chem.* **2000**, *39*, 2206.
(18) Personov, R. I. In *Spectroscopy and Excitation Dynamics of Condensed Molecular Systems*; Agranovich, V. M., Hochstrasser, R. M., Eds.; North-Holland: Amsterdam, The Netherlands, 1983; pp 555−619.
(19) Riesen, H.; Krausz, E. *Chem. Phys. Lett.* **1990**, *172*, 5.
(20) (a) Szabo, A.; Kaarli, R. *Phys. Rev. B* **1991**, *44*, 12307. (b) Riesen, H.; Hayward, B. F.; Szabo, A. *J. Lumin.* **2007**, *127*, 655.
(21) Riesen, H.; Krausz, E.; Dubicki, L. *Chem. Phys. Lett.* **1994**, *218*, 579.
(22) Singer, L. S. *J. Chem. Phys.* **1955**, *23*, 379.
(23) McGarvey, B. R. *J. Chem. Phys.* **1964**, *40*, 809.
(24) Kennedy, J. M.; Schäffer, C. E. *Inorg. Chim. Acta* **1996**, *252*, 185.
(25) Dubicki, L.; Bramley, R. *Chem. Phys. Lett.* **1997**, *272*, 55.
(26) *Spartan 04*; Wavefunction Inc.: Irvine, CA, 2004.

JP805831A